Electrochimica Acta 369 (2021) 137677

Contents lists available at ScienceDirect

Electrochimica Acta

journal homepage: www.elsevier.com/locate/electacta

Densely packed open microspheres by soft template electropolymerization of benzotrithiophene-based monomers

Yanis Levieux-Souid[a], Ananya Sathanikan[a], François Orange[b], Frédéric Guittard[a], Thierry Darmanin[a,*]

[a] Université Côte d'Azur, NICE Lab, 06200 Nice, France
[b] Université Côte d'Azur, Centre Commun de Microscopie Appliquée (CCMA), 06100 Nice, France

ARTICLE INFO

Article history:
Received 10 October 2020
Revised 22 December 2020
Accepted 22 December 2020
Available online 27 December 2020

Keywords:
Nanostructures
Template
Conducting polymer
Wettability
Hydrophobicity

ABSTRACT

Here, a soft electropolymerization approach (called templateless) is used to prepare extremely ordered porous surface structures. For the first time, benzotrithiophene-based monomers are chosen for their high aromaticity and exceptional electropolymerization capacity. Different parameters are tested such as the nature of the substituent, the presence of a ketone group between the monomer and the substituent, the water content and the electropolymerization method. Homogeneous structures are especially obtained without ketone group, probably because the ketone group reduces π-stacking interactions between benzotrithiophene moieties. Unique results are obtained with the monomers with aromatic groups (phenyl and naphthalene), which lead to densely packed huge open spheres by cyclic voltammetry and in dichloromethane saturated with water. Here, just a phenyl group is sufficient compared to other works with 3,4-phenylenedioxythiophene (PheDOT), 3,4-naphthalenedioxythiophene (NaphDOT) and thieno[3,4-*b*]thiophene because BTT is already extremely aromatic. These porous surfaces could be used is the future for a huge number of applications such as in water-harvesting systems, oil adsorbents, sensors or is drug delivery.

1. Introduction

Extremely controlled porous nanostructures have been explored for a wide range of applications for example in catalyst, sensors, adsorbents, drug delivery or for their wetting properties [1–7] In Nature, the wetting properties are omnipresent (gecko toepads, plant, wing surfaces,…) and is fundamental to well-adjust both the surface energy and surface structures [8–11]. It was demonstrated that vertically aligned nanotubes are an excellent choice for their surface-area-to-volume ratio allowing to control the wetting properties and their dimensions (diameter, height, porosity, shape) [12,13].

Their formation on substrates often needs complex and long processes, typically using hard templates [14,15]. The templateless electropolymerization is an excellent candidate to prepare ordered surface structures very quickly, but also with tunable shape (nanotubes, nanocaps…) [14–26]. In this process, gas bubbles are formed on the substrate during electropolymerization and are used as soft template. For example, pyrrole was extensively studied in the literature directly in water (H_2O) and in the presence of surfactant [14–20]. During electropolymerization, H_2O can be oxidized or reduced to produce O_2 and H_2 bubbles which are stabilized by the surfactant and allowing the polymer growth around the gas bubbles.

However, most of the monomers are not soluble in H_2O while the electropolymerization in H_2O often needs high monomer concentration. It was recently reported that this soft template electropolymerization is possible in organic solvent such as dichloromethane (CH_2Cl_2) if H_2O is present in solution in order to form H_2/O_2 bubbles [21–26]. It is even possible without surfactant if the monomer can stabilize the gas bubbles. Highly rigid and aromatic thiophene-base molecules such as PheDOT, NaphDOT and thienothiophene derivatives gave exceptional results such as vertically aligned nanotubes, nanorings or coral-like structures.

In this work, we investigate for the first time extremely aromatic and conjugated thiophene-base molecules called benzotrithiophene (BTT), known for their exceptional electropolymerization capacity and optoelectronic properties [27–30]. Here, BTT was chosen as monomer because it was demonstrated that molecules favoring π-sticking interactions such as NaphDOT or pyrene seem to be excellent choices [21,22,31]. The two series studied are represented in Scheme 1. Both the influence of the

* Corresponding author.
E-mail address: thierry.darmanin@unice.fr (T. Darmanin).

https://doi.org/10.1016/j.electacta.2020.137677
0013-4686/

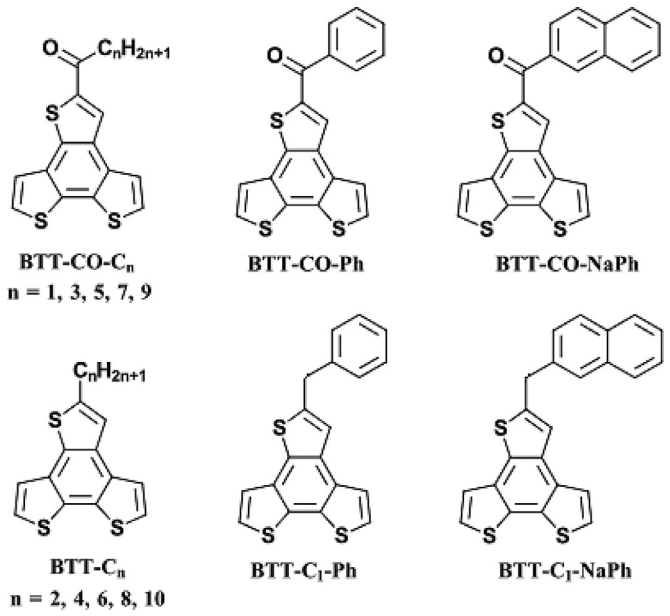

Scheme 1. Benzotrithiophene based monomers investigated in the manuscript.

substituent (various linear alkyl chains and aromatic groups) as well as the presence of a ketone group between the monomer and the substituent on the resulting surface structures and hydrophobicity are studied. Because it was reported that the presence of H_2O has a huge influence on the formation of porous structures and especially on their number [25], two solvents are studied CH_2Cl_2 and CH_2Cl_2 saturated with H_2O called here CH_2Cl_2 + H_2O.

2. Materials and method

2.1. Monomer synthesis

The synthesis way is schematized in Scheme 2. Monomers were synthesized in four steps from 2,3-dibromothiophene, adjusting a procedure reported in the literature.[27] ^1H and ^{13}C NMR spectra are available in Supporting Information.

For the first reaction, to an ice-cooled solution of 2,3-dibromothiophene (10.0 g, 0.0413 mol) and the corresponding acid chloride (1,2 eq., 0.049 mol) in anhydrous dichloromethane (200 mL) was added aluminum chloride (8.26 g, 0.062 mol) portion-wise during 15 min. The reaction mixture was stirred for 24 h and then quenched with ice-cold hydrochloric acid (1 M, 50 mL) and water (50 mL). The quenched reaction mixture was extracted with chloroform and dried over anhydrous sodium sulphate and concentrated to afford the crude product. Purification by column chromatography (silica gel, 80/20: cyclohexane/chloroform).

2,3-Dibromo-5-acetylthiophene: Yield 50%; oily Yellow-Orange solid; ^1H NMR (200 MHz, $CDCl_3$) δ 7.47 (s, 1H), 2.51 (s, 3H).

2,3-Dibromo-5-butyrylthiophene: Yield 48%; oily Yellow-Orange solid; ^1H NMR (300 MHz, $CDCl_3$) δ 7.47 (s, 1H), 2.80 (t, J = 7.2 Hz, 2H), 1.70 (m, 2H), 0.92 (t, J = 7.4 Hz, 3H).

2,3-Dibromo-5-hexanoylthiophene: Yield 86%; oily Yellow-Orange solid; ^1H NMR (200 MHz, $CDCl_3$) δ 7.46 (s, 1H), 2.79 (t, J = 7.2 Hz, 2H), 1.71 (m, 2H), 1.34 (m, 2H), 0.89 (t, J = 6.7 Hz, 3H).

2,3-Dibromo-5-octanoylthiophene: Yield 40%; oily Yellow-Orange solid; ^1H NMR (300 MHz, $CDCl_3$) δ 7.49 (s, 1H), 2.82 (t, J = 7.2 Hz, 2H), 1.73 (m, 2H), 1.32 (m, 6H), 0.89 (t, J = 6.7 Hz, 3H).

2,3-Dibromo-5-decanoylthiophene: Yield 70%; oily Yellow-Orange solid ^1H NMR (300 MHz, $CDCl_3$) δ 7.49 (s, 1H), 2.82 (t, J = 7.2 Hz, 2H), 1.73 (m, 2H), 1.30 (m, 10H), 0.87 (t, J = 6.7 Hz, 3H).

2,3-Dibromo-5-benzoylthiophene: Yield 83%; oily Yellow-Orange solid; ^1H NMR (300 MHz, $CDCl_3$) δ 7.82 (m, 2H), 7.57 (m, 3H), 7.42 (s, 1H).

2,3-Dibromo-5-naphtanoylthiophene: Yield 58%; oily Yellow-Orange solid;^1H NMR (300 MHz, $CDCl_3$) δ 8.38 (s, 1H), 7.97 (m, 4H), 7.58 (m, 3H).

For the second step, a suspension of **1** (1 eq), thiophene-3-boronic acid (2.2 eq) and sodium carbonate (4,24 g) was prepared in toluene (60 mL), ethanol (10 mL) and water (20 mL). Then, tetrakis(triphenylphosphine)palladium(0) (0.069 eq) was added and the reaction mixture was heated at 100 °C to reflux for 24 h. The solvents were evaporated. After purification by column chromatography (silica gel, 50/50: cyclohexane/chloroform), the crude product obtained was mainly an intermediate product. A suspension of this intermediate product (1 eq), thiophene-3-boronic acid (2.2 eq) and sodium carbonate (4,24 g) in toluene

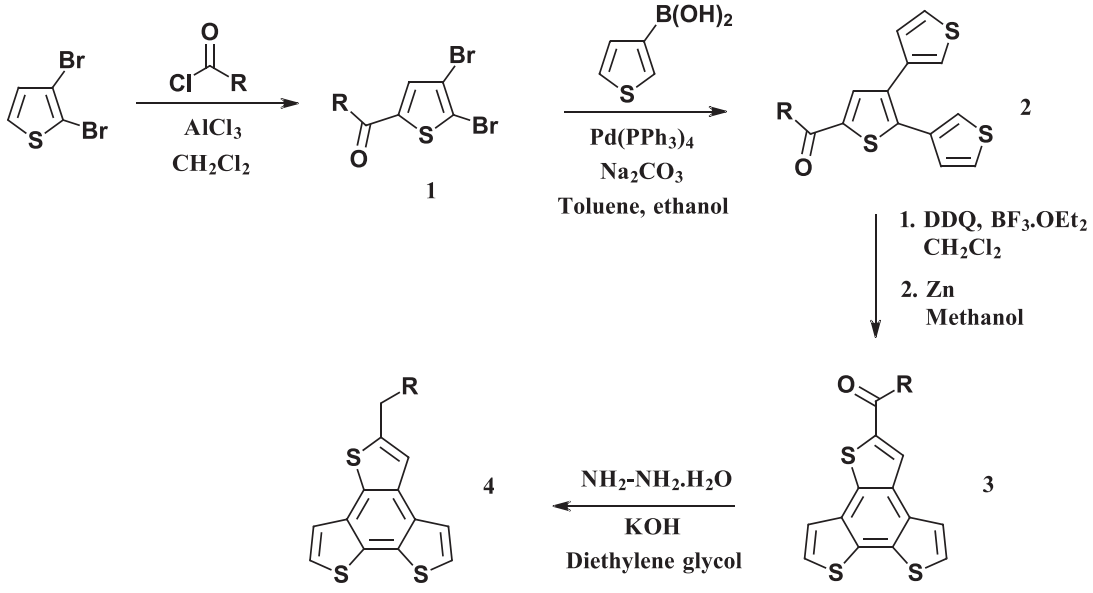

Scheme 2. Chemical route to the monomers.

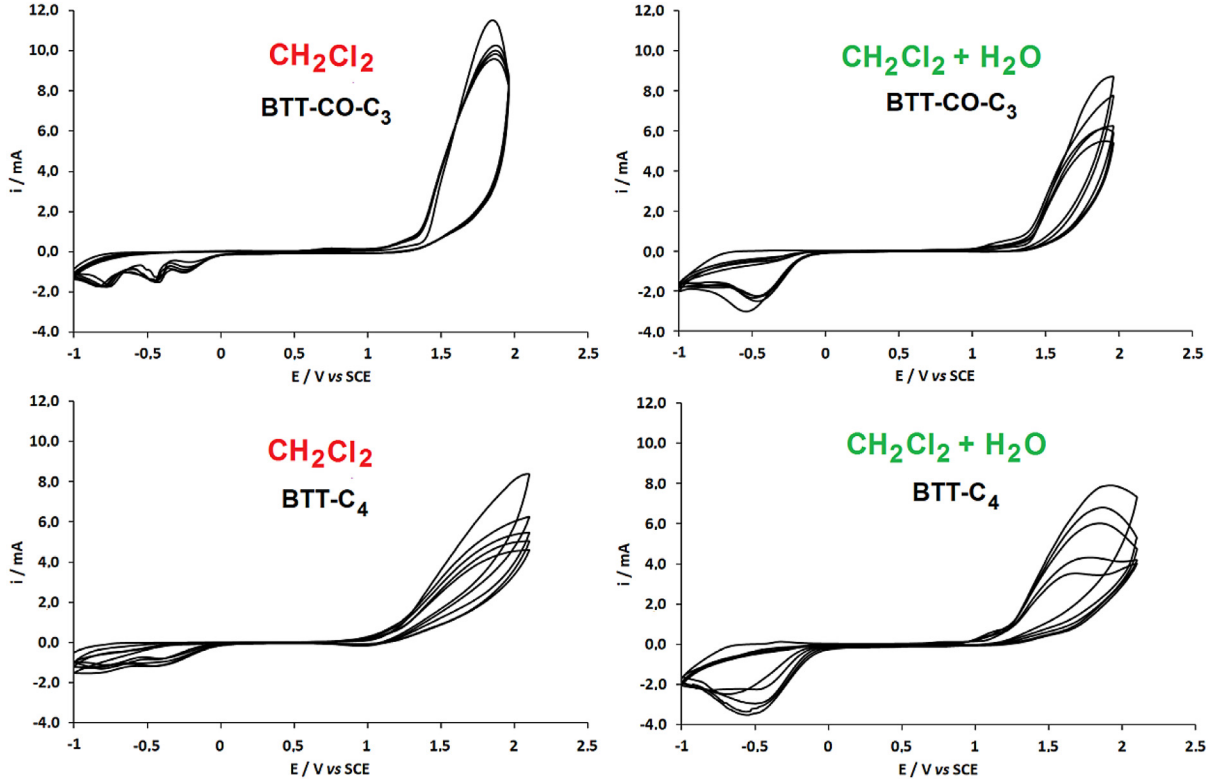

Fig. 1. Electropolymerization of BTT-CO-C_3 and BTT-C_4 (10 mM) by cyclic voltammetry (5 scans) in 0.1 M Bu_4NClO_4 / CH_2Cl_2 (left) and CH_2Cl_2 + H_2O (right) at a scan rate of 20 mV s^{-1}.

(20 mL), ethanol (20 mL) and water (20 mL) was performed again. Then tetrakis(triphenylphosphine)palladium(0) (0.069 eq) was added and the reaction mixture was heated at 100 °C to reflux for 24 h. Then, the solvents were evaporated. Purification by column chromatography (silica gel, 50/50: cyclohexane /chloroform).

5-Acetyl-2,3-bis(3-thienyl)thiophene: Yield 18%; pale yellow solid ^{1}H NMR (300 MHz, $CDCl_3$) δ 7.69 (s, 1H), 7.29 (m, 3H), 7.26 (dd, J = 3.0 Hz, J = 1.3 Hz, 1H), 7.00 (m, 2H), 2.59 (s, 3H).

5-Butyryl-2,3-bis(3-thienyl)thiophene: Yield 21%; pale yellow solid ^{1}H NMR (300 MHz, $CDCl_3$) δ 7.70 (s, 1H), 7.28 (m, 3H), 7.24 (dd, J = 3.0 Hz, J = 1.3 Hz, 1H), 7.01 (m, 2H), 2.89 (t, J = 7.3 Hz, 2H), 1.80 (m, 2H), 1.00 (t, J = 7.4 Hz, 3H).

5-Hexanoyl-2,3-bis(3-thienyl)thiophene: Yield 44%; pale yellow solid ^{1}H NMR (300 MHz, $CDCl_3$) δ 7.70 (s, 1H), 7.28 (m, 3H), 7.25 (dd, J = 3.0 Hz, J = 1.3 Hz, 1H), 7.00 (m, 2H), 2.89 (t, J = 7.4 Hz, 2H), 1.78 (m, 2H), 1.39 (m, 4H), 0.93 (t, J = 7.0 Hz, 3H).

5-Octanoyl-2,3-bis(3-thienyl)thiophene: Yield 27%; pale yellow solid ^{1}H NMR (300 MHz, $CDCl_3$) δ 7.68 (s, 1H), 7.28 (m, 3H), 7.21 (dd, J = 3.0 Hz, J = 1.3 Hz, 1H), 7.00 (m, 2H), 2.88 (t, J = 7.4 Hz, 2H), 1.76 (m, 2H), 1.32 (m, 6H), 0.88 (t, J = 6.7 Hz, 3H).

5-Decanoyl-2,3-bis(3-thienyl)thiophene: Yield 29%; pale yellow solid ^{1}H NMR (300 MHz, $CDCl_3$) δ 7.67 (s, 1H), 7.30 (m, 3H), 7.21 (dd, J = 3.0 Hz, J = 1.3 Hz, 1H), 7.00 (m, 2H), 2.92 (t, J = 7.4 Hz, 2H), 2.86 (m, 2H), 1.25 (m, 8H), 0.87 (t, J = 6.7 Hz, 3H).

5-Benzoyl-2,3-bis(3-thienyl)thiophene: Yield 49%; pale yellow solid ^{1}H NMR (300 MHz, $CDCl_3$) δ 7.93 (m, 2H), 7.67 (s, 1H), 7.55 (m, 3H), 7.35 (m, 3H), 7.25 (dd, J = 3.0 Hz, J = 1.4 Hz, 1H), 7.07 (dd, J = 4.9 Hz, J = 1.4 Hz, 1H), 7.02 (dd, J = 4.9 Hz, J = 1.4 Hz, 1H).

5-Naphtanoyl-2,3-bis(3-thienyl)thiophene: Yield 43%; pale yellow solid ^{1}H NMR (300 MHz, $CDCl_3$) 8.47 (s, 1H), 8.00 (m, 4H), 7.74 (s, 1H), 7.63 (m, 3H), 7.38 (m, 3H), 7.26 (dd, J = 2.9 Hz, J = 1.2 Hz, 1H),7.09 (dd, J = 4.9 Hz, J = 1.2 Hz, 1H), 7.04 (dd, J = 4.9 Hz, J = 1.4 Hz, 1H).

For the third step, to an ice-cooled solution of **2** (1 eq) in anhydrous dichloromethane (140 mL) was added boron trifluoride diethyl etherate (1.3 eq) after which 2,3-dichloro-5,6-dicyano-1,4-benzoquinone (1.2 eq) was added portion wise for 10 min. The reaction mixture was allowed to warm to room temperature for 48 h and was subsequently quenched by addition of zinc (7.7 eq) and methanol (70 mL). After stirring overnight, the reaction mixture was filtered, washed with chloroform, dried over anhydrous sodium sulphate and concentrated to afford the crude product. Purification by column chromatography (silica gel, 50/50: cyclohexane/chloroform).

BTT-CO-C_1: Yield 16%; White solid; m.p. 162.5 °C; ^{1}H NMR (300 MHz, $CDCl_3$) δ 8.13 (s, 1H), 7.60 (d, J = 5.4 Hz, 1H), 7.48 (d, J = 5.4 Hz, 1H), 7.43 (d, J = 5.4 Hz, 1H), 7.40 (d, J = 5.4 Hz, 1H), 2.62 (s, 3H); ^{3}C NMR (75 MHz, $CDCl_3$) δ 191.76, 142.09, 136.47, 133.22, 132.19, 131.09, 127.96, 125.54, 125.37, 122.64, 122.43, 26.89.

BTT-CO-C_3: Yield 82%; White solid; m.p. 155.0 °C; ^{1}H NMR (300 MHz, $CDCl_3$) δ 8.32 (s, 1H), 7.76 (d, J = 5.4 Hz, 1H), 7.63 (d, J = 5.4 Hz, 1H), 7.55 (d, J = 5.4 Hz, 1H), 7.53 (d, J = 5.4 Hz, 1H), 3.06 (t, J = 7.2 Hz, 2H), 1.89 (m, 2H), 1.08 (t, J = 7.4 Hz, 3H); ^{13}C NMR (75 MHz, $CDCl_3$) δ 194.35, 142.13, 136.22, 133.56, 133.26, 132.25, 131.68, 131.17, 127.13, 125.50, 125.32, 122.66, 122.48, 41.25, 18.28, 13.93.

BTT-CO-C_5: Yield 23%; White solid; m.p. 78.2 °C; ^{1}H NMR (300 MHz, $CDCl_3$) δ 8.30 (s, 1H), 7.72 (d, J = 5.4 Hz, 1H), 7.62 (d, J = 5.4 Hz, 1H), 7.54 (d, J = 5.4 Hz, 1H), 7.52 (d, J = 5.4 Hz, 1H), 3.06 (t, J = 7.2 Hz, 1H), 1.88 (m, 2H), 1.41 (t, J = 6.4 Hz, 5H), 0,93 (m,3H); ^{13}C NMR (75 MHz, $CDCl_3$) 194.50, 142.09, 136.20, 133.26, 132.24, 131.15, 127.11, 125.51, 125.32, 122.68, 122.51, 39.38, 31.57, 24.54, 22.55, 13.99.

BTT-CO-C_7: Yield 47%; White solid; m.p. 81.1 °C; ^{1}H NMR (300 MHz, $CDCl_3$ δ 8.03 (s, 1H), 7.52 (d, J = 5.4 Hz, 1H), 7.41 (m, 3H), 2.97 (t, J = 7.4 Hz, 2H), 1.80 (m, 2H), 1.34 (m, 8H), 0,90 (t, J = 6.0 Hz, 3H); ^{13}C NMR (75 MHz, $CDCl_3$) 194.20, 141.78, 135.78,

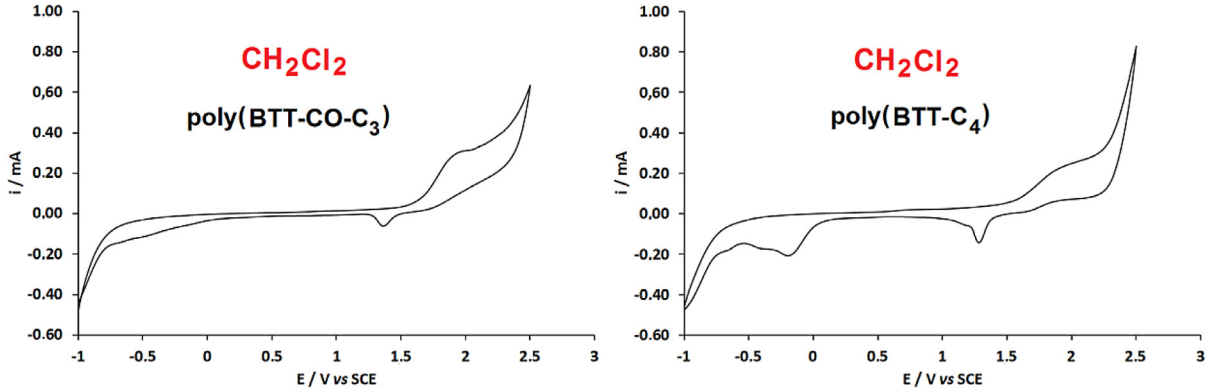

Fig. 2. Cyclic voltammogram of electrodeposited surfaces obtained from BTT-CO-C_3 and BTT-C_4 in 0.1 M Bu_4NClO_4 / CH_2Cl_2 at a scan rate of 20 mV s^{-1}.

133.15, 132.91, 131.84, 131.26, 130.79, 126.72, 125.17, 124.93, 122.38, 122.31, 39.29, 31.79, 31.73, 29.43, 29.36, 29.24, 29.15, 24.74, 22.72, 14.19.

BTT-CO-C_9: Yield 25%; White solid; m.p. 78.5 °C; ^{1}H NMR (300 MHz, $CDCl_3$) δ 8.12 (s, 1H), 7.60 (d, J = 5.4 Hz, 1H), 7.49 (m, 3H), 3.03 (t, J = 7.4 Hz, 2H), 1.84 (m, 2H), 1.31 (t, 12H), 0,93 (t, J = 6.7 Hz, 3H); ^{13}C NMR(75 MHz, $CDCl_3$) 194.35, 141.95, 136.00, 133.36, 133.10, 132.05, 131.47, 130.99, 126.90, 125.33, 125.11, 122.53, 122.41, 39.37, 31.92, 29.54, 29.45, 29.34, 26.94, 24.81, 22.71, 14.16.

BTT-CO-Ph: Yield 45%; White solid; m.p. 171.4 °C; ^{1}H NMR (300 MHz, $CDCl_3$) δ 8.19 (s, 1H), 7.96 (m, 2H), 7.62 (m, 5H), 7.50 (d, J = 5.4 Hz, 1H), 7.48 (d, J = 5.4 Hz, 1H); ^{13}C NMR (75 MHz, $CDCl_3$) 189.14, 141.28, 138.13, 136.71, 133.72, 133.28, 132.44, 132.18, 131.72, 131.02, 130.47, 129.30, 128.62, 125.56, 125.32, 122.70, 122.57.

BTT-CO-NaPh: Yield 40%; White solid; No m.p.; ^{1}H NMR (300 MHz, $CDCl_3$) δ 8.52 (s, 1H), 8.31 (s, 1H), 8.00 (m, 4H), 7.72 (d, J = 5.4 Hz, 1H), 7.70 (d, J = 5.4 Hz, 1H), 7.62 (m, 2H), 7.56 (d, J = 5.4 Hz, 1H), 7.54 (d, J = 5.4 Hz, 1H); ^{13}C NMR (75 MHz, $CDCl_3$) 189.13, 141.44, 136.74, 135.41, 135.23, 133.76, 133.45, 133.40, 133.33, 133.17, 132.38, 132.24, 131.08, 130.53, 129.38, 128.60, 128.31, 127.90, 127.83, 127.02, 126.97, 125.60, 125.35, 122.74, 122.61.

For the fourth step, to a suspension of **3** (1 eq) in ethylene glycol (10 mL) was added hydrazine monohydrate (50 eq) and potassium hydroxide (30 eq) and the reaction mixture was stirred at 190 °C overnight. The cooled reaction mixture was poured into water, extracted with chloroform, dried over sodium sulphate and concentrated to afford the crude product. Purification was performed by column chromatography (silica gel, 50/50: cyclohexane/chloroform).

BTT-C_2: Yield 74%; White solid; m.p. 103.2 °C; ^{1}H NMR (300 MHz, $CDCl_3$) δ 7.69 (d, 5.4 Hz, 1H), 7.56 (d, J = 5.4 Hz, 1H), 7.48 (d, J = 5.4 Hz, 1H), 7.46 (d, J = 5.4 Hz, 1H), 7.43 (t, J = 1.1 Hz, 1H), 3.07 (m, 2H), 1.44 (t, J = 7.2 Hz, 3H); ^{13}C NMR (75 MHz, $CDCl_3$) δ 146.84, 132.88, 132.41, 131.52, 130.95, 130.82, 129.82, 124.79, 124.08, 122.76, 122.32, 118.69, 24.12, 15,83.

BTT-C_4: Yield 40%; White solid; m.p. 43.8 °C; ^{1}H NMR (300 MHz, $CDCl_3$ δ 7.69 (d, 5.4 Hz, 1H), 7.55 (d, J = 5.4 Hz, 1H), 7.48 (d, J = 5.4 Hz, 1H), 7.46 (d, J = 5.4 Hz, 1H), 7.42 (t, J = 1.0 Hz, 1H), 3.01 (t, J = 7.5 Hz, 2H), 1.81 (m, 2H), 1.50 (m, 2H), 0.99 (t, J = 7.3 Hz, 3H). ^{13}C NMR (75 MHz, $CDCl_3$) δ 145.30, 132.83, 132.34, 131.48, 131.01, 130.78, 129.76, 124.77, 124.05, 122.75, 122.29, 119.37, 33.61, 30.43, 22.20, 13.84.

BTT-C_6: Yield 51%; White solid; m.p. 42.8 °C; ^{1}H NMR (300 MHz, $CDCl_3$ δ 7.69 (d, 5.4 Hz, 1H), 7.56 (d, J = 5.4 Hz, 1H), 7.48 (d, J = 5.4 Hz, 1H), 7.46 (d, J = 5.4 Hz, 1H), 7.42 (t, J = 0.9 Hz, 1H), 3.01 (t, J = 7.5 Hz, 2H), 2.03 (m, 2H), 1.82 (m, 2H) 1.36 (m, 4H), 0.94 (t, J = 7.2 Hz, 3H). ^{13}C NMR (75 MHz, $CDCl_3$) 145.36, 132.84, 132.31, 131.49, 129.76, 124.75, 124.03, 122.74, 122.27, 119.37, 31.62, 31.50, 30.91, 30.76, 28.82, 22.59, 14.10.

Table 1
Monomer and polymer oxidation potential.

Monomer	$E^{ox}_{monomer}$ [V *vs* SCE]	$E^{ox}_{polymer}$ [V *vs* SCE]
BTT-CO-C_1	2.27	1.90
BTT-CO-C_3	1.96	1.96
BTT-CO-C_5	1.96	1.89
BTT-CO-C_7	2.05	1.92
BTT-CO-C_9	2.10	1.91
BTT-CO-Ph	2.27	1.91
BTT-CO-NaPh	2.33	1.91
BTT-C_2	2.12	1.99
BTT-C_4	2.10	1.95
BTT-C_6	2.10	1.99
BTT-C_8	2.00	1.98
BTT-C_{10}	1.95	1.95
BTT-C_1-Ph	2.20	1.95
BTT-C_1-NaPh	2.36	2.00

BTT-C_8: Yield 43%; White solid; m.p. 45.2 °C; δ 7.68 (d, 5.4 Hz, 1H), 7.54 (d, J = 5.4 Hz, 1H), 7.47 (d, J = 5.4 Hz, 1H), 7.45 (d, J = 5.4 Hz, 1H), 7.41 (t, J = 0.9 Hz, 1H), 2.95 (t, J = 7.3 Hz, 2H), 1.90 (m, 2H), 1.20 (m, 10H), 0.85 (t, J = 6.6 Hz, 3H); ^{13}C NMR (75 MHz, $CDCl_3$) 145.39, 132.87, 132.38, 131.52, 124.78, 124.05, 122.78, 122.32, 119.39, 77.69, 77.05, 76.42, 31.91, 31.58, 30.80, 29.42, 29.27, 29.19, 22.71, 14.15.

BTT-C_{10}: Yield 40%; Liquid; ^{1}H NMR (200 MHz, $CDCl_3$); δ 7.69 (d, 5.4 Hz, 1H), 7.55 (d, J = 5.4 Hz, 1H), 7.48 (d, J = 5.4 Hz, 1H), 7.46 (d, J = 5.4 Hz, 1H), 7.42 (t, J = 0.9 Hz, 1H), 3.00 (t, J = 7.4 Hz, 2H), 1.90 (m, 2H), 1.30 (m, 16H), 0.85 (t, J = 6.2 Hz, 3H); ^{13}C NMR (75 MHz, $CDCl_3$) 145.41, 124.79, 124.06, 122.78, 122.32, 119.40, 77.66, 77.03, 76.39, 31.92, 31.56, 30.79, 29.62, 29.58, 29.42, 29.35, 29.15, 22.70, 14.13.

BTT-C_1-Ph: Yield 41%; White solid; m.p. 120.8 °C; ^{1}H NMR (200 MHz, $CDCl_3$) δ 7.65 (d, J = 5.4 Hz, 1H), 7.50 (d, J = 5.4 Hz, 1H), 7.46 (m, 3H), 7.37 (m, 4H), 4.33 (s, 2H); ^{13}C NMR (75 MHz, $CDCl_3$) 131.44, 128.76, 128.71, 126.79, 124.89, 124.20, 122.78, 122.30, 120.64, 102.96, 77.65, 77.33, 77.21, 77.18, 77.02, 76.84, 76.79, 76.62, 76.38, 36.94.

BTT-C_1-NaPh: Yield 67%; White solid; m.p. 150.4 °C; ^{1}H NMR (300 MHz, $CDCl_3$) δ 7.86 (m, 4H), 7.65 (d, J = 5.4 Hz, 1H), 7.48 (m, 7H), 4.50 (s, 2H); ^{13}C NMR (75 MHz, $CDCl_3$) 143.73, 137.26, 133.61, 132.76, 132.45, 132.42, 131.85, 131.44, 130.93, 130.10, 128.35, 127.71, 127.20, 127.10, 126.21, 125.72, 124.90, 124.21, 122.79, 122.30, 120.84, 37.11.

Table 2
Arithmetic (Ra) and quadratic (Rq) surfaces roughness, surface area (for an analysed surface of 0.275 mm^2) and roughness parameter (r) of Wenzel equation, for the surfaces obtained by cyclic voltammetry in CH_2Cl_2 + H_2O.

Monomer	Number of deposition scans	Ra [μm]	Rq [μm]	Surface area [mm^2]	r
BTT-CO-C_1	1	1.6 ± 0.3	2.6 ± 0.4	0.872	3.2
	3	*	*	*	*
	5	*	*	*	*
BTT-CO-C_3	1	0.15 ± 0.04	0.42 ± 0.10	0.291	1.1
	3	0.63 ± 0.05	1.0 ± 0.13	0.361	1.3
	5	0.70 ± 0.13	1.0 ± 0.16	0.433	1.6
BTT-CO-C_5	1	0.07 ± 0.02	0.08 ± 0.03	0.275	1.0
	3	0.13 ± 0.02	0.20 ± 0.04	0.275	1.0
	5	0.87 ± 0.08	1.0 ± 0.17	0.702	2.6
BTT-CO-C_7	1	0.07 ± 0.02	0.15 ± 0.2	0.275	1.0
	3	0.56 ± 0.07	0.84 ± 0.12	0.390	1.4
	5	1.6 ± 0.2	2.2 ± 0.25	0.480	1.7
BTT-CO-Ph	1	2.1 ± 0.3	4.2 ± 0.4	0.600	2.2
	3	4.2 ± 0.7	5.5 ± 0.9	0.840	3.1
	5	*	*	*	*
BTT-CO-NaPh	1	0.90 ± 0.01	1.2 ± 0.2	0.510	1.9
	3	*	*	*	*
	5	*	*	*	*
BTT-C_2	1	0.92 ± 0.25	1.2 ± 0.3	0.529	1.9
	3	1.5 ± 0.2	2.0 ± 0.2	0.812	2.9
	5	1.8 ± 0.2	2.3 ± 0.3	0.925	3.4
BTT-C_4	1	0.84 ± 0.04	1.3 ± 0.1	0.780	2.8
	3	1.8 ± 0.3	2.4 ± 0.40	0.947	3.4
	5	1.8 ± 0.2	2.4 ± 0.35	0.763	2.8
BTT-C_6	1	0.08 ± 0.01	0.12 ± 0.02	0.275	1.0
	3	0.23 ± 0.04	0.30 ± 0.05	0.280	1.0
	5	1.46 ± 0.16	2.0 ± 0.30	0.581	2.1
BTT-C_8	1	0.14 ± 0.02	230 ± 35	0.277	1.0
	3	1.6 ± 0.2	2.0 ± 0.20	0.750	2.7
	5	1.45 ± 023	1.90 ± 0.25	0.801	2.9
BTT-C_{10}	1	0.22 ± 0.05	0.32 ± 0.07	0.281	1.0
	3	1.2 ± 0.2	1.8 ± 0.28	0.600	2.2
	5	1.5 ± 0.22	2.0 ± 0.30	0.606	2.2
BTT-C_1-Ph	1	0.78 ± 0.10	1.1 ± 0.11	0.495	1.8
	3	*	*	*	*
	5	*	*	*	*
BTT-C_1-NaPh	1	0.30 ± 0.09	0.45 ± 0.11	0.283	1.0
	3	*	*	*	*
	5	*	*	*	*

*too rough for the optical profilometry.

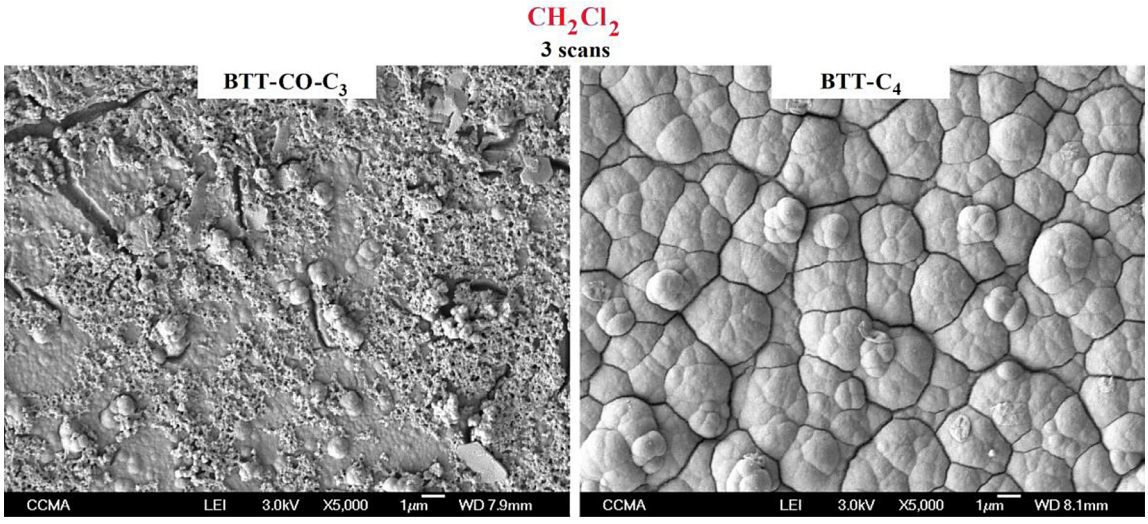

Fig. 3. SEM images obtained with BTT-CO-C_3 and BTT-C_4 in CH_2Cl_2. 3 scans at a scan rate of 20 mV s^{-1}.

2.2. Soft template electropolymerization

The soft electropolymerization experiments were realized with a potentiostat (Autolab from Metrohm) *via* three electrodes: 2 cm^2 gold-silicon wafer as the working electrode, a glassy carbon rod as the counter-electrode and a saturated calomel electrode (SCE) as the reference electrode. Tetrabutylammonium perchlorate (Bu_4NClO_4) was used as the supporting electrolyte with a concentration of 0.1 M. Two solvents were tested CH_2Cl_2 and CH_2Cl_2 + H_2O. CH_2Cl_2 + H_2O was prepared by mixing CH_2Cl_2 with a high amount of H_2O and discarding the aqueous phase. The depositions were performed either by cyclic voltammetry (1, 3 and 5

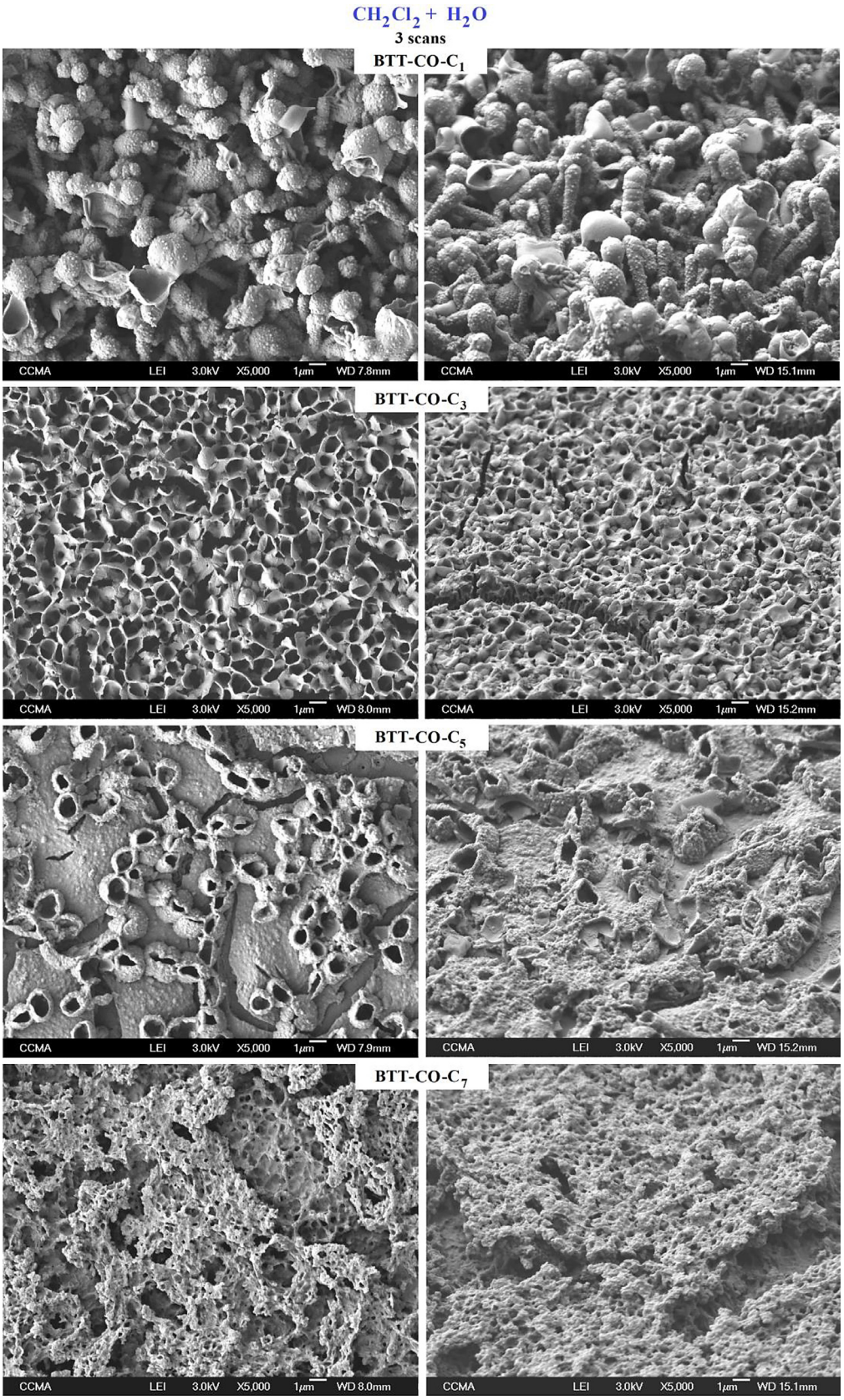

Fig. 4. SEM images obtained with BTT-CO-C_1, BTT-CO-C_3, BTT-CO-C_5 and BTT-CO-C_7 in CH_2Cl_2 + H_2O. 3 scans at a scan rate of 20 mV s^{-1}. The substrates are not inclined (on the left) and inclined at 45° (on the right).

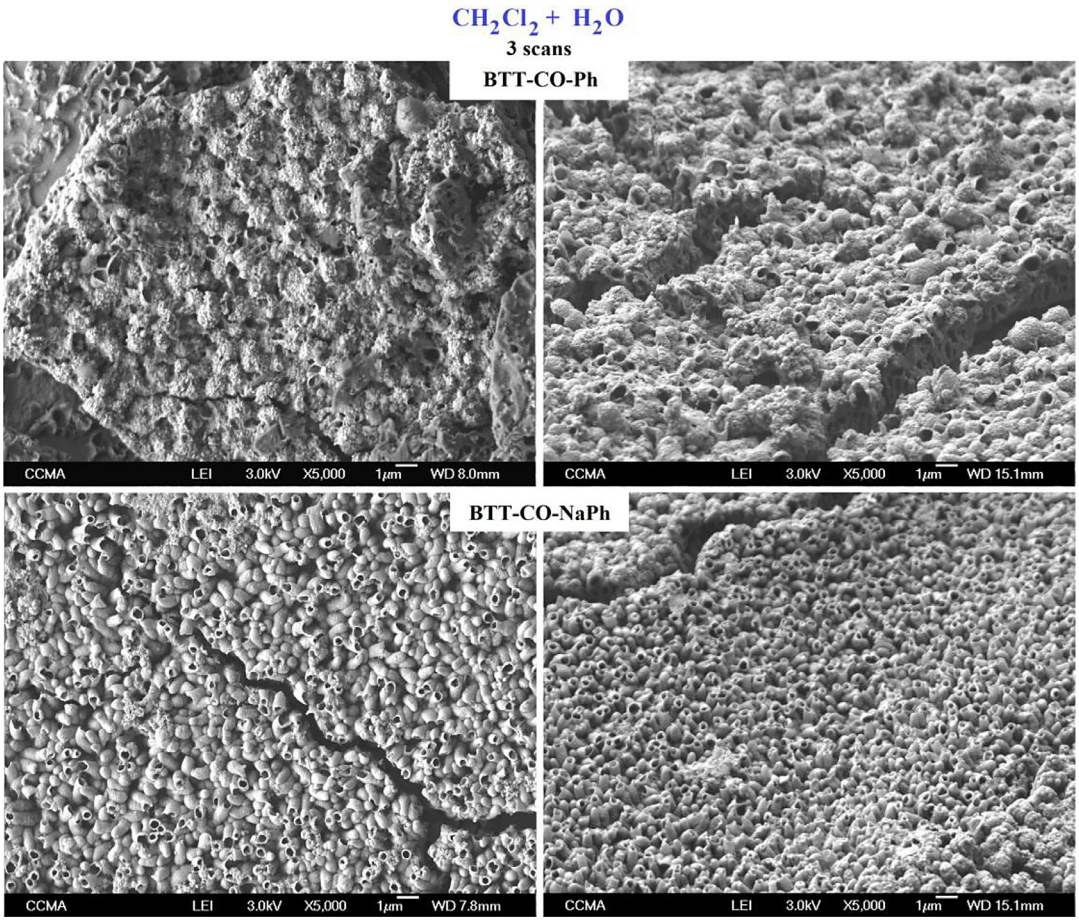

Fig. 5. SEM images obtained with BTT-CO-Ph and BTT-CO-NaPh in CH_2Cl_2 + H_2O. 3 scans at a scan rate of 20 mV s^{-1}. The substrates are not inclined (on the left) and inclined at 45° (on the right).

scans at a scan rate of 20 mV s^{-1}) or at constant potential (12.5, 25, 50, 100, 200 and 400 mC cm^{-2} at a potential of the monomer oxidation potential E^{ox}).

Smooth surfaces were also prepared in CH_2Cl_2 at constant potential and using an ultra-short deposition charge of 1 mC cm^{-2}. Then, the polymers were reduced by cyclic voltammetry: 1 back scan from E^{ox} to −1 V.

2.3. Surface characterization

After metallization, surfaces structures were imaged *via* scanning electron microscopy (SEM) (6700F microscope from JEOL) without and with a substrate inclination of 45°. The surface hydrophobicity was characterized *via* goniometer (DSA30 from Bruker) with 2 μL water droplets and by measuring the apparent contact angles with water (θ_w) taken at the triple point (n = 5). IR spectra were performed on a Spectrum 100 FT-IR spectrometer (Perkin Elmer, USA) with a diamond attenuated total reflectance (ATR) top plate accessory. A Tescan Vega 3 XMU scanning electron microscope equipped with an X-MaxN 50 EDX detector was used for the EDX analyses. The arithmetic (Ra) and quadratic (Rq) roughness were obtained with a WYKO NT1100 optical profiling system from Bruker using the objective 20X, and the field of view 0.5X (analysed surface of 0.275 mm^2). The white light vertical scanning Interferometry (VSI) was used for the surfaces with low roughness and the red light High Mag Phase Shift Interferometry (PSI) was used for the surfaces with high roughness.

Table 3
Wettability data for the polymer films obtained by cyclic voltammetry (3 scans in CH_2Cl_2 + H_2O at the san rate of 20 mV s^{-1}.

Monomer	θ_w [deg]
BTT-CO-C_1	34.0 ± 11.3
BTT-CO-C_3	67.5 ± 2.1
BTT-CO-C_5	97.8 ± 3.7
BTT-CO-C_7	72.1 ± 3.1
BTT-CO-C_9	74.8 ± 2.9
BTT-CO-Ph	66.2 ± 4.4
BTT-CO-NaPh	109.4 ± 16.6
BTT-C_2	91.6 ± 10.3
BTT-C_4	52.7 ± 0.3
BTT-C_6	90.6 ± 3.2
BTT-C_8	65.0 ± 11.0
BTT-C_{10}	72.7 ± 3.9
BTT-C_1-Ph	76.1 ± 6.5
BTT-C_1-NaPh	94.8 ± 16.5

3. Results and discussion

In this work, in agreement to previous works [25], two solvents were tested for soft template electropolymerization: CH_2Cl_2 and CH_2Cl_2 saturated with H_2O (CH_2Cl_2 + H_2O). As reported in literature, the formation of H_2 bubbles from H_2O (2 H_2O + 2 e^- → **H_2** (bubbles) + 2 OH^-) is perfectly visible by cyclic voltammetry at ≈ −0.5 V *vs* SCE during the back scan, but only for CH_2Cl_2 + H_2O.

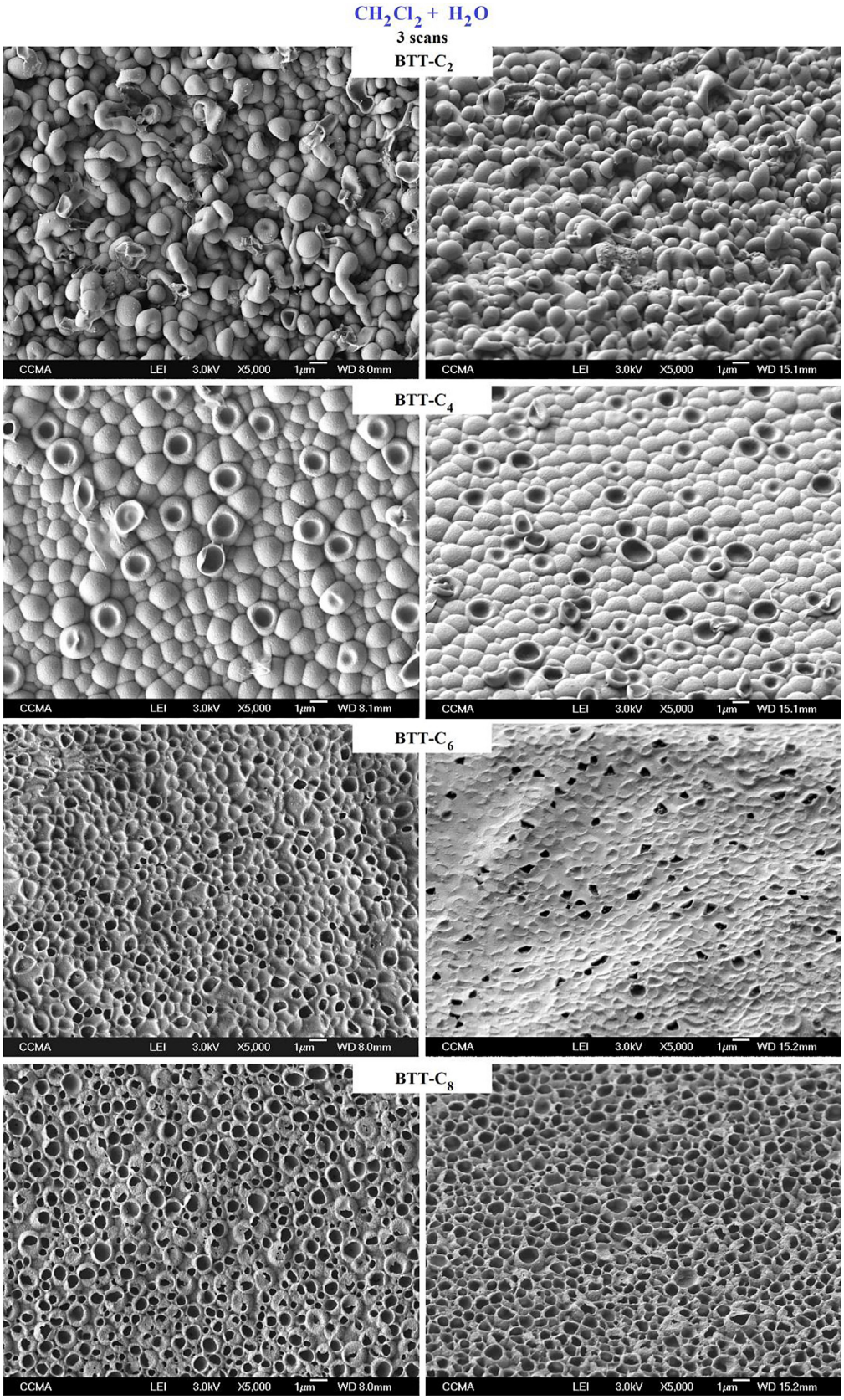

Fig. 6. SEM images obtained with BTT-C_2, BTT-C_4, BTT-C_6 and BTT-C_8 in $CH_2Cl_2 + H_2O$. 3 scans at a scan rate of 20 mV s^{-1}. The substrates are not inclined (on the left) and inclined at 45° (on the right).

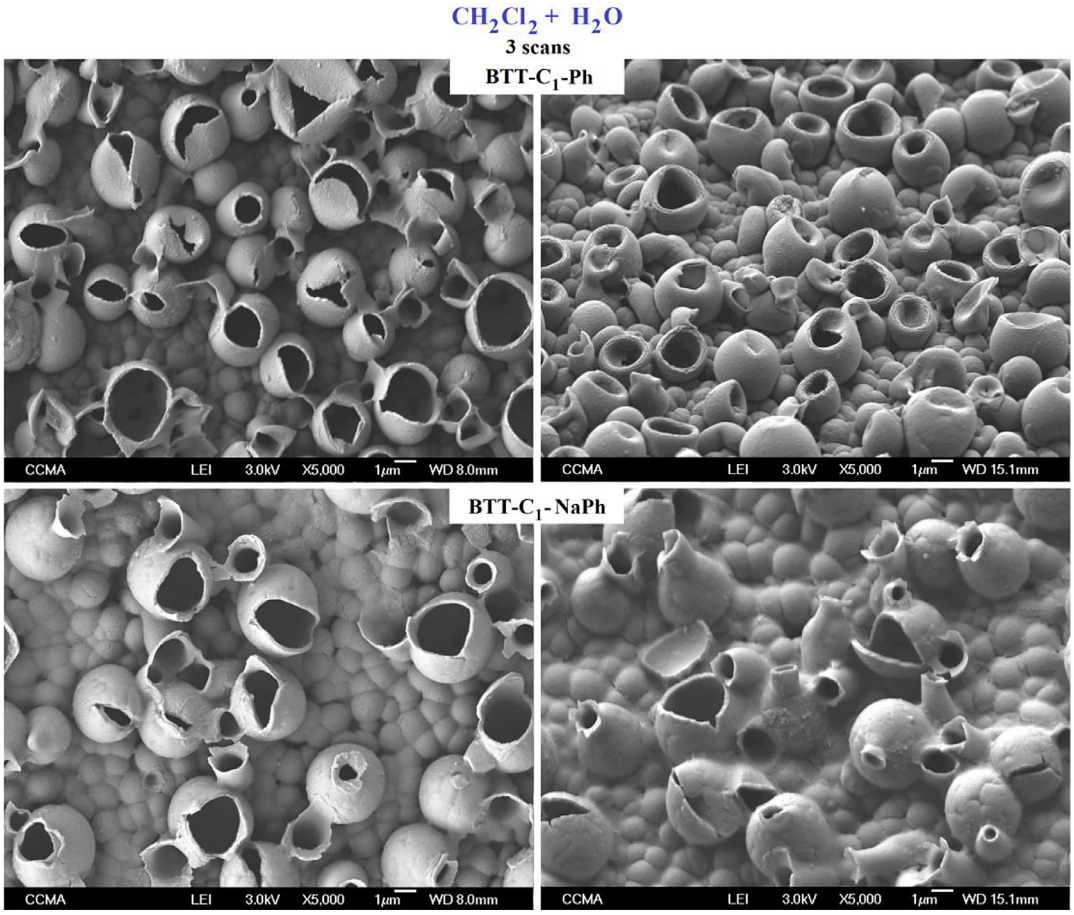

Fig. 7. SEM images obtained with BTT-C_1-Ph and BTT-C_1-NaPh in CH_2Cl_2 + H_2O. 3 scans at a scan rate of 20 mV s^{-1}. The substrates are not inclined (on the left) and inclined at 45° (on the right).

Table 4
Young's angles and surface energy for the smooth polymer films.

Monomer	$\theta_{Y,w}$ [deg]	$\theta_{Y,diiodo}$ [deg]	$\theta_{Y,hexad}$ [deg]	$\gamma_{S,P}$	$\gamma_{S,D}$	γ_S
BTT-CO-C_1	61.0 ± 1.0	36.0 ± 4.3	0	15.5	29.4	44.9
BTT-CO-C_3	63.9 ± 1.1	31.2 ± 3.1	0	14.4	30.5	44.9
BTT-CO-C_5	61.8 ± 2.6	26.9 ± 5.8	0	15.6	31.0	46.6
BTT-CO-C_7	66.7 ± 2.1	28.4 ± 3.9	0	12.6	31.2	43.8
BTT-CO-C_9	66.2 ± 2.4	28.8 ± 1.9	0	12.9	31.1	44.0
BTT-CO-Ph	61.2 ± 3.5	21.6 ± 2.4	0	15.6	31.7	47.3
BTT-CO-NaPh	59.4 ± 5.8	33.4 ± 2.7	0	17.6	29.6	47.2
BTT-C_2	60.1 ± 1.7	24.0 ± 5.0	0	16.5	31.2	47.7
BTT-C_4	66.4 ± 2.6	33.6 ± 5.5	0	13.1	30.3	43.4
BTT-C_6	68.4 ± 4.4	26.5 ± 2.1	0	11.5	31.7	43.2
BTT-C_8	70.5 ± 3.3	22.3 ± 4.6	0	10.1	32.5	42.6
BTT-C_{10}	65.4 ± 6.8	27.1 ± 1.4	0	13.3	31.3	44.6
BTT-C_1-Ph	61.6 ± 1.0	27.0 ± 4.1	0	17.8	30.6	48.4
BTT-C_1-NaPh	64.3 ± 3.9	24.8 ± 1.7	0	13.8	31.5	45.3

Another peak is also present during the forward scan, indicative of the reaction 2 $H_2O \rightarrow$ **O_2** (bubbles) + 4 H^+ + 4 e^- but starts only at ≈ 2.0 V.

Then, the monomers were added and their oxidation potential (E^{ox}) was found to be both depending on the substituent and the presence of ketone (Table 1). Then, cyclic voltammetry (from −1 V to E^{ox}) was chosen as the electropolymerization method. It is expected especially the release of H_2 bubbles during the back scans but also a lower amount of O_2 bubbles during the forward scans.

Examples of cyclic voltammograms in CH_2Cl_2 are given in Fig. 1. The polymer surfaces were also electrochemically characterized in solutions free of monomers in order to better determine the oxidation and reduction potentials (Fig. 2 and Supporting Information). For example, the oxidation potential of the polymer surfaces in very close to that of the monomer (Table 2) and the effect of the substituent is slight (1.89 $V < E^{ox}_{polymer} < 2.00$ V). These results are similar to that obtained monomers highly favouring π-stacking interactions such as with pyrene-based monomers, for which the coatings containing both ultra-short oligomers and monomer [32–34].

In CH_2Cl_2 + H_2O, the cyclic voltammograms are relatively close expected the presence of a very intense peak between 0 and −1 V

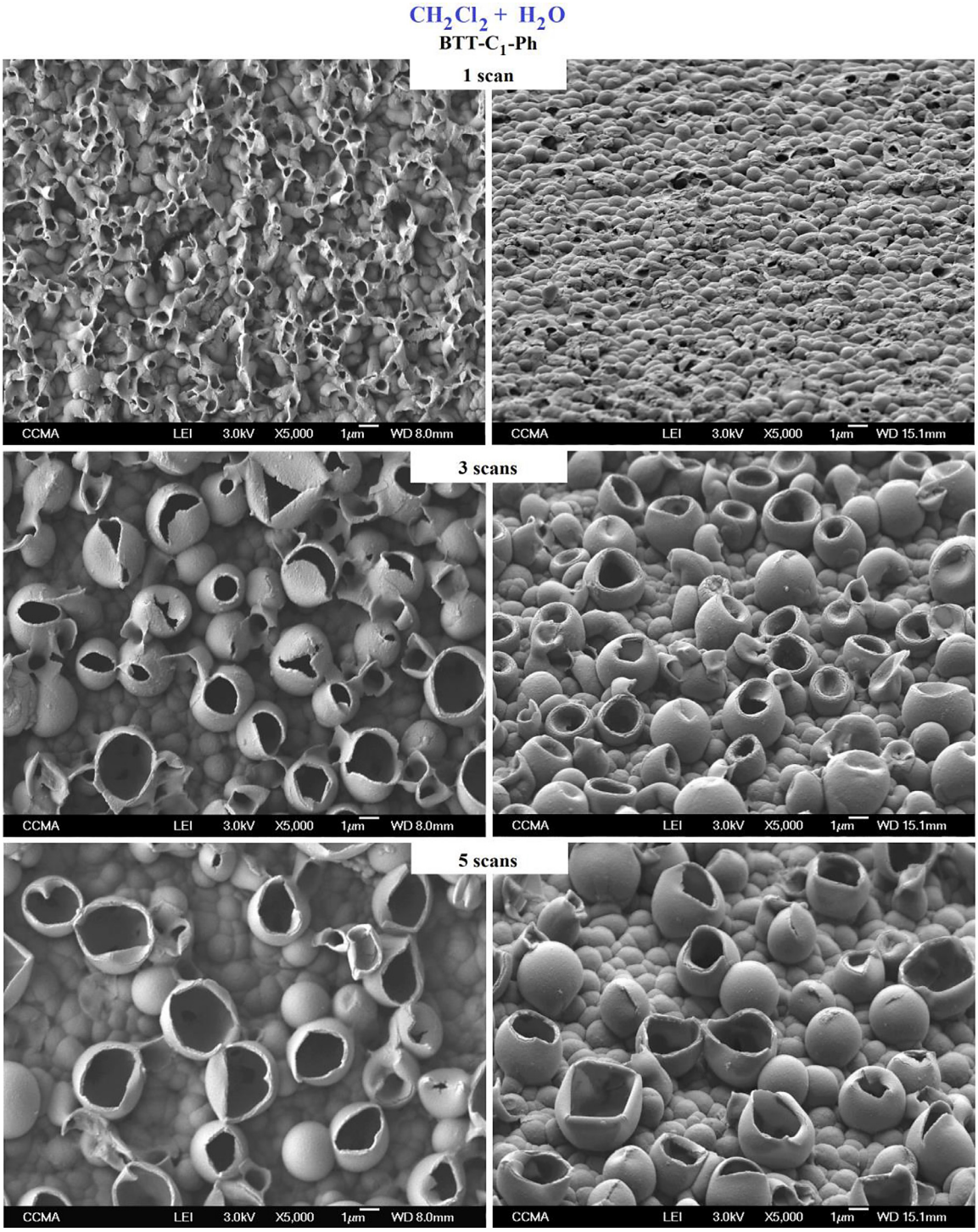

Fig. 8. SEM images obtained with BTT-C_1-Ph in CH_2Cl_2 + H_2O. 1, 3 and 5 scans at a scan rate of 20 mV s^{-1}. The substrates are not inclined (on the left) and inclined at 45° (on the right).

only during the back scans confirming the release of H_2 bubbles from H_2O.

For the effects on the surface structures, first the influence of the solvent (CH_2Cl_2 or CH_2Cl_2 + H_2O) was studied by SEM using only **BTT-CO-C_3** and **BTT-C_4**. In CH_2Cl_2, the surfaces obtained with **BTT-CO-C_3** have a low roughness, are inhomogeneous and with some nanoparticles (Fig. 3). With **BTT-C_4**, the surfaces are homogeneous with huge microdomes even if no open structures such as nanotubes are observed. It is worth noting that electrodeposition of unsubstituted **BTT** was already reported in literature [35–37] in anhydrous CH_2Cl_2 and acetonitrile, and the presence of nanofibers was observed especially in CH_2Cl_2 [35].

By contrast, the surfaces obtained in CH_2Cl_2 + H_2O contain a much higher number of porous structures (Fig. 3). Therefore, the effect of the substituent and the presence of ketone was performed especially in CH_2Cl_2 + H_2O. Here, also the surfaces obtained with the monomers with ketone groups are not extremely homogeneous (Figs. 4 and 5). The monomer with an ultra-short alkyl chain **BTT-CO-C_1** leads to a huge number of vertically aligned tubules but most of the tubes formed are close. Then, the in-

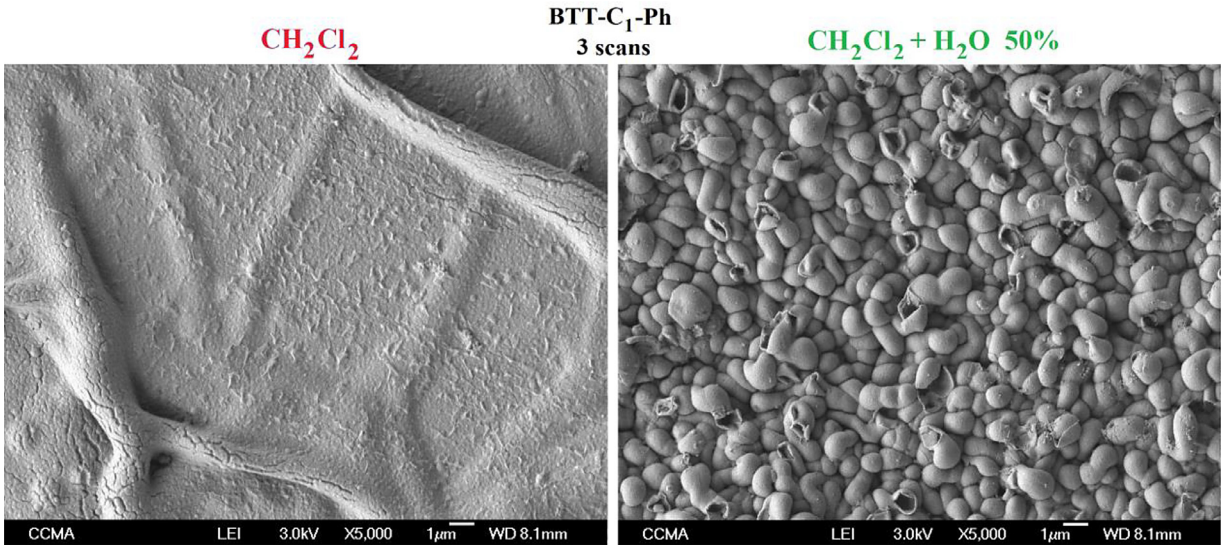

Fig. 9. SEM images obtained with BTT-C_1-Ph in CH_2Cl_2 and CH_2Cl_2 + H_2O 50%. 3 scans at a scan rate of 20 mV s^{-1}.

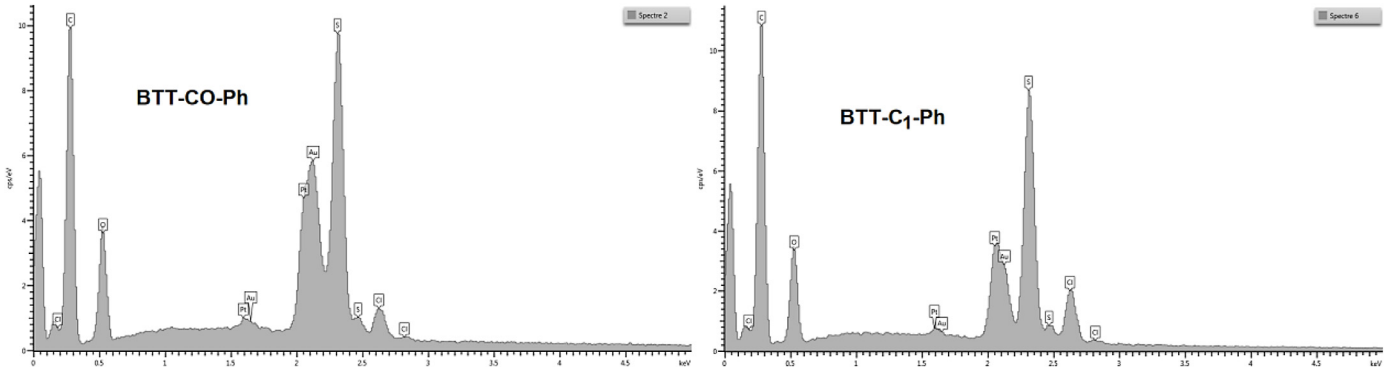

Fig. 10. EDX spectra of polymer surfaces obtained with BTT-C_1-Ph and BTT-CO-Ph in Bu_4NClO_4 / CH_2Cl_2 + H_2O. 3 scans at a scan rate of 20 mV s^{-1}.

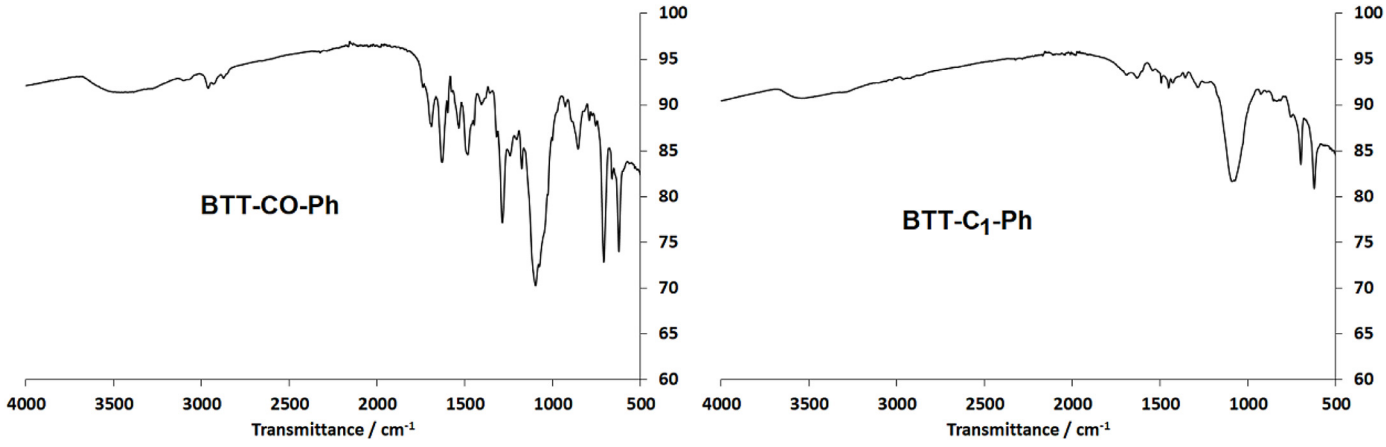

Fig. 11. IR spectra of polymer surfaces obtained with BTT-C_1-Ph and BTT-CO-Ph in Bu_4NClO_4 / CH_2Cl_2 + H_2O. 3 scans at a scan rate of 20 mV s^{-1}.

crease in the alkyl chain length changes the surfaces structures from close nanotubules to nanoporous membranes (**BTT-CO-C_3**) and after the porosity decreases with the alkyl chain length. With aromatic groups (**BTT-CO-Ph** and **BTT-CO-NaPh**) nanotubules are formed but with **BTT-CO-NaPh** the majority of the tubes formed are open and the surfaces are more homogeneous.

By contrast, extremely homogeneous surfaces are obtained with the monomers without ketone confirming the importance to do the ketone reduction (Figs. 6 and 7). Both spherical, tubular and close structures are observed with ultra-short alkyl chain **BTT-C_2** but their height is relatively small. Then, a change from spherical structures to nanoporous membrane is also observed as a function of the alkyl chain length passing through nanorings with **BTT-C_4**.

Unique results are obtained with aromatic groups (**BTT-C_1-Ph, BTT-C_1-NaPh**) as already reported in the literature with thieno [3,4-*b*]thiophene derivatives, for example (Fig. 6). Densely packed huge open spheres are formed with these monomers. Their mean diameter is roughly ≈ 2–3 μm and their thickness ≈ 0.5 μm. The

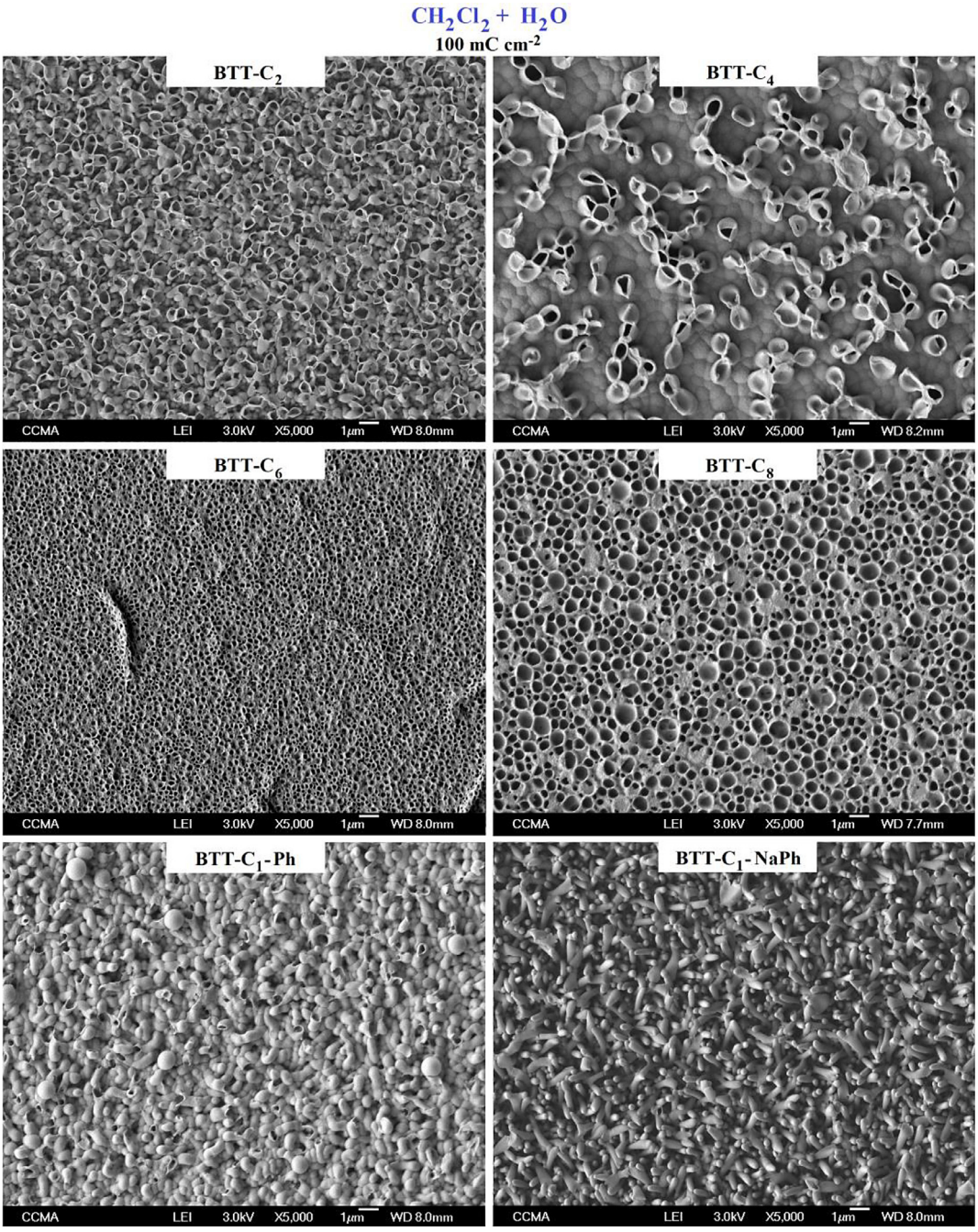

Fig. 12. SEM images obtained with BTT-C_2, BTT-C_4, BTT-C_6, BTT-C_8, BTT-C_1-Ph and BTT-C_1-NaPh in CH_2Cl_2 + H_2O. 100 mC cm^{-2}.

study as a function of the number of scans (Fig. 8) shows that more than 1 scan are necessary to produce these huge spheres confirming the necessity to release of high amount of gas. Here, the polymer growth is clearly three-dimensional (3D). Compared to previous works [21,23,32,33], densely packed hollows were never reported compared to vertically aligned nanotubes, even if thieno [3,4-*b*]thiophene derivatives with pyrene substituents gave relatively close results but less ordered. Moreover, just a phenyl group is sufficient compared to other works with PheDOT, NaphDOT and thieno [3,4-*b*]thiophene because benzotrithiophene is already extremely aromatic.

Hence, the presence of a ketone group leads to less ordered surfaces. This fundamental result may be explained by a decrease of interactions (especially π-stacking) between benzotrithiophene moieties. Indeed, it was demonstrated that even the position of the substituent can highly affect the polymer growth [24].

In order to better estimate the influence of H_2O content, **BTT-C_1-Ph** was electropolymerized not only in CH_2Cl_2 but also in CH_2Cl_2 + H_2O diluted 50% *vs* CH_2Cl_2, called CH_2Cl_2 + H_2O 50%. SEM images (Fig. 9) show that in CH_2Cl_2 the surfaces are relatively smooth with just some wrinkles while in CH_2Cl_2 + H_2O 50% the surfaces contain spheres of smaller size and most of them are close.

The surfaces were characterized by optical profilometry to determine their surface roughness, surface area as well as the roughness parameter (r) of the Wenzel equation [40] (Table 2). By cyclic voltammetry, the surface roughness is extremely high even after just one deposition scan, which is expected due to the release of

Table 5
Wettability data for the polymer films obtained at constant potential from BTT-C_1–NaPh.

Deposition charge [mC cm^{-2}]	θ_w [deg]
12.5	73.1 ± 1.1
25	94.0 ± 5.9
50	99.6 ± 5.0
100	94.4 ± 3.2
200	64.0 ± 5.8
400	0

a high amount of H_2 bubbles. After one deposition scan, the highest roughness is obtained with **BTT-CO-Ph** and **BTT-CO-C_1** and the lowest roughness with **BTT-CO-C_5, BTT-CO-C_7** and **BTT-C_8**.

The surfaces were also chemically characterized by EDX and infrared. The EDX analyses (Fig. 10) show for the substrate the presence of Au (95.3 mass%), C (4.2 mass%) and O (0.5 mass%). It was not possible to distinguish the monomers with or without ketone because it is observed the presence of remaining perchlorate (ClO_4^-) counterions. For example, for **BTT-C_1-Ph** it was found C (52.2 mass %), O (10.3 mass %), S (19.3 mass %), Cl (2.6 mass %) and Au (15.6 mass %) while for **BTT-CO-Ph** there is C (63.3 mass %), O (11.4 mass %), S (17.9 mass %), Cl (5.0 mass %) and Au (2.4 mass %). For the IR spectra, peaks are present for example at ≈ 2800–3000 cm^{-1} for C–H stretching, 1500–1700 cm^{-1} for C=C stretching, 1100–1300 cm^{-1} for C–S stretching and C=C bending (Fig. 11).

The study of their surface hydrophobicity shows that θ_w is extremely varied with a maximum of 109.4° for **BTT-CO-NaPh** (Table 3). The surfaces with densely packed huge open spheres obtained with **BTT-C_1-Ph** are slightly hydrophilic and it is observed a slight increase of θ_w with the number of deposition scans.

In order to better explain the wettability results, it was very important to prepare smooth polymers. Table 4 shows that all these smooth polymers are intrinsically hydrophilic whatever the substituent with Young's angle [38] with water $59.4° < \theta_{Y,w} < 70.5°$ and surface energy, determined with the Owens Wendt equation [39], 42.6 mN $m^{-1} < \gamma_S <$ 48.4 mN m^{-1}. The monomers without ketone often leads to more hydrophobic surfaces, as expected due to its high polarity. The hydrophobicity increases with the alkyl chain length until n = 8 and decreases after because the surface becomes saturated. **BTT-C_1-NaPh** leads also to more hydrophobic surfaces than **BTT-C_1-Ph**.

Using all the monomers without ketone, another deposition method is also tested: the deposition at constant potential ($E = E^{ox}$). In this method, only O_2 bubbles can be released even if their number should be low because the monomer oxidation potential is close to that of H_2O. SEM images for a deposition charge (Qs) of 100 mC cm^{-2} are gathered in Fig. 12. Here, nanotubular structures and nanoporous surfaces are also mainly observed.

Using **BTT-C_1-NaPh**, vertically aligned nanotubes are formed (Fig. 13). With this electrodeposition method, it is observed the presence of nanopores for Qs = 12.5 mC cm^{-2} before the formation of nanotubes. Most of the tubes are open with short Qs up to 50 mC cm^{-2}. Then, the nanotubes become close at higher Qs. Moreover, it is also observed an increase in the size of the tubes with Qs. For the wetting properties (Table 5), it is also observed an increase of θ_w up to 99.6° for Qs = 50 mC cm^{-2} and a decrease after because the nanotubes became close. Hence, when a droplet is on a surface made with Qs = 50 mC cm^{-2}, the amount of air between the surface and a water droplet is the highest because it is energetically difficult to wet inside the open nanotubes even if the material is intrinsically hydrophilic. This is an intermediate state between the Wenzel and the Cassie-Baxter state [40–45].

At constant potential, the surfaces surface roughness and surface area are given in Table 6. Here, the surfaces are less rough

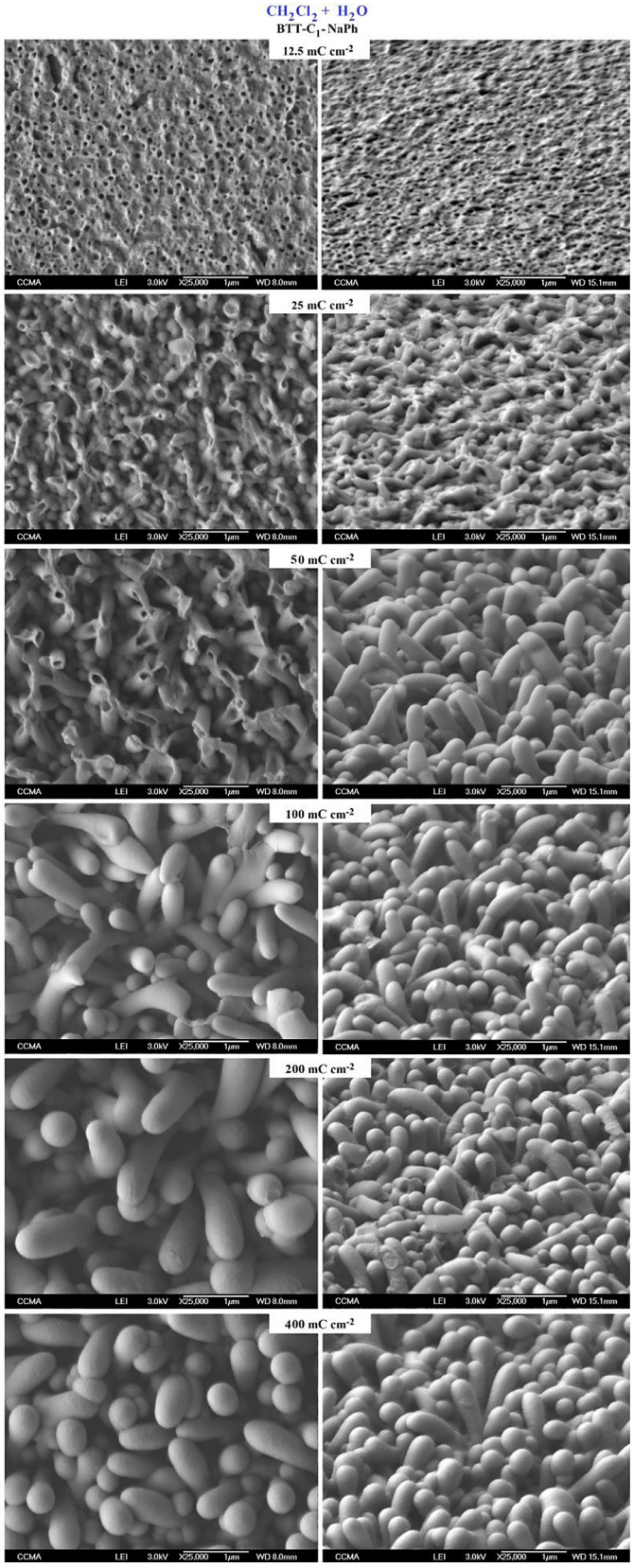

Fig. 13. SEM images obtained with BTT-C_1-NaPh in CH_2Cl_2 + H_2O from 12.5 to 400 mC cm^{-2}.

Table 6
Arithmetic (Ra) and quadratic (Rq) surfaces roughness, surface area (for an analysed surface of 0.275 mm^2) and roughness parameter (r) of Wenzel equation, for the surfaces obtained at constant potential in CH_2Cl_2+ H_2O.

Monomer	Number of deposition charge [mC cm^{-2}]	Ra [μm]	Rq [μm]	Surface area [mm^2]	r
BTT-CO-C_1	12.5	0.02 ± 0.01	0.03 ± 0.01	0.275	1.0
	25	0.03 ± 0.01	0.04 ± 0.01	0.275	1.0
	50	0.05 ± 0.01	0.06 ± 0.01	0.275	1.0
	100	0.37 ± 0.05	0.58 ± 0.09	0.360	1.3
	200	0.52 ± 0.10	0.74 ± 0.12	0.432	1.6
	400	1.0 ± 0.1	2.1 ± 0.2	0.667	2.4
BTT-CO-C_3	12.5	0.07 ± 0.01	0.10 ± 0.01	0.275	1.0
	25	0.08 ± 0.02	0.17 ± 0.03	0.275	1.0
	50	0.08 ± 0.02	0.13 ± 0.02	0.275	1.0
	100	0.26 ± 0.04	0.42 ± 0.10	0.315	1.2
	200	0.40 ± 0.05	0.54 ± 0.09	0.391	1.4
	400	0.68 ± 0.12	0.90 ± 0.15	0.431	1.6
BTT-CO-C_5	12.5	0.03 ± 0.01	0.04 ± 0.01	0.275	1.0
	25	0.04 ± 0.01	0.06 ± 0.01	0.275	1.0
	50	0.04 ± 0.01	0.05 ± 0.01	0.275	1.0
	100	0.24 ± 0.05	041 ± 0.12	0.390	1.4
	200	0.42 ± 0.09	0.76 ± 0.16	0.330	1.2
	400	1.2 ± 0.2	1.7 ± 0.3	0.620	2.3
BTT-CO-C_7	12.5	0.02 ± 0.01	0.03 ± 0.01	0.275	1.0
	25	0.02 ± 0.01	0.03 ± 0.01	0.275	1.0
	50	0.05 ± 0.01	0.06 ± 0.01	0.275	1.0
	100	1.4 ± 0.1	1.8 ± 0.2	0.958	3.5
	200	1.5 ± 0.1	2.1 ± 0.2	1.16	4.2
	400	2.4 ± 0.3	3.1 ± 0.4	1.10	4.0
BTT-CO-Ph	12.5	0.03 ± 0.01	0.06 ± 0.01	0.275	1.0
	25	0.04 ± 0.01	0.06 ± 0.01	0.275	1.0
	50	0.10 ± 0.02	0.14 ± 0.03	0.275	1.0
	100	0.49 ± 0.06	0.60 ± 0.09	0.341	1.2
	200	0.94 ± 0.20	1.4 ± 0.3	0.466	1.7
	400	1.6 ± 0.4	2.4 ± 0.6	0.702	2.6
BTT-CO-NaPh	12.5	0.02 ± 0.03	0.04 ± 0.01	0.275	1.0
	25	0.04 ± 0.01	0.05 ± 0.01	0.275	1.0
	50	0.04 ± 0.01	0.05 ± 0.01	0.275	1.0
	100	0.21 ± 0.02	0.29 ± 0.03	0.281	1.0
	200	0.21 ± 0.02	0.31 ± 0.03	0.281	1.0
	400	0.35 ± 0.04	0.45 ± 0.05	0.290	1.1
BTT-C_2	12.5	0.04 ± 0.01	0.06 ± 0.01	0.275	1.0
	25	0.05 ± 0.01	0.07 ± 0.01	0.275	1.0
	50	0.05 ± 0.01	0.07 ± 0.01	0.275	1.0
	100	0.12 ± 0.03	0.15 ± 0.04	0.275	1.0
	200	0.10 ± 0.02	0.13 ± 0.02	0.275	1.0
	400	0.24 ± 0.04	0.30 ± 0.06	0.282	1.0
BTT-C_4	12.5	0.04 ± 0.01	0.05 ± 0.01	0.275	1.0
	25	0.03 ± 0.01	0.05 ± 0.01	0.275	1.0
	50	0.06 ± 0.01	0.07 ± 0.01	0.275	1.0
	100	0.24 ± 0.04	0.46 ± 0.05	0.320	1.2
	200	0.38 ± 0.06	0.63 ± 0.08	0.444	1.6
	400	0.42 ± 0.8	0.75 ± 0.13	0.521	1.9
BTT-C_6	12.5	0.05 ± 0.01	0.06 ± 0.01	0.275	1.0
	25	0.05 ± 0.01	0.09 ± 0.01	0.275	1.0
	50	0.06 ± 0.01	0.09 ± 0.01	0.275	1.0
	100	0.14 ± 0.02	0.48 ± 0.03	0.300	1.1
	200	0.23 ± 0.05	0.47 ± 0.10	0.343	1.2
	400	1.8 ± 0.3	2.9 ± 0.5	1.00	3.6
BTT-C_8	12.5	0.02 ± 0.01	0.04 ± 0.01	0.275	1.0
	25	0.03 ± 0.01	0.04 ± 0.01	0.275	1.0
	50	0.03 ± 0.01	0.06 ± 0.01	0.275	1.0
	100	0.44 ± 0.08	0.75 ± 0.09	0.301	1.1
	200	1.7 ± 0.1	2.2 ± 0.2	1.12	4.1
	400	1.9 ± 0.1	2.5 ± 0.2	1.15	4.2
BTT-C_{10}	12.5	0.02 ± 0.01	0.02 ± 0.01	0.275	1.0
	25	0.04 ± 0.01	0.06 ± 0.01	0.275	1.0
	50	0.05 ± 0.01	0.06 ± 0.01	0.275	1.0
	100	0.05 ± 0.01	0.06 ± 0.01	0.275	1.0
	200	1.0 ± 0.1	1.3 ± 0.2	0.430	1.6
	400	1.4 ± 0.1	1.8 ± 0.2	0.835	3.0
BTT-C_1-Ph	12.5	0.04 ± 0.01	0.05 ± 0.01	0.275	1.0
	25	0.05 ± 0.01	0.06 ± 0.01	0.275	1.0
	50	0.05 ± 0.01	0.07 ± 0.01	0.275	1.0
	100	0.15 ± 0.04	0.20 ± 0.04	0.281	1.0
	200	0.56 ± 0.10	1.2 ± 0.2	0.437	1.6
	400	0.83 ± 0.15	1.3 ± 0.2	0.510	1.9
BTT-C_1-NaPh	12.5	0.03 ± 0.01	0.04 ± 0.01	0.275	1.0
	25	0.04 ± 0.01	0.05 ± 0.01	0.275	1.0
	50	0.05 ± 0.01	0.07 ± 0.01	0.275	1.0
	100	0.40 ± 0.05	0.51± 0.08	0.305	1.1
	200	0.30 ± 0.06	0.39 ± 0.05	0.306	1.1
	400	0.33 ± 0.05	0.44 ± 0.09	0.292	1.1

than the surfaces by cyclic voltammetry because only small amount of O_2 bubbles can be released. An increase of the surface roughness is observed but especially after from 100 mC cm^{-2}. After 400 mC cm^{-2}, the lowest roughness is observed with **BTT-CO-NaPh, BTT-C_2, BTT-C_4** and **BTT-C_1-NaPh**.

Conclusion

In this original work, we investigated benzotrithiophene-based monomers by soft template electropolymerization. We have shown how to obtain extremely ordered porous surface structures of different shape. We tested different parameters such as the nature of the substituent, the presence of a ketone group between the monomer and the substituent, the water content and the electropolymerization method. Unique results are obtained with the monomers without ketone and with aromatic substituents (phenyl and naphthalene), which lead to densely packed huge open spheres by cyclic voltammetry and in dichloromethane saturated with water. These surfaces could be used for a wide range of applications such as in water harvesting systems, drug delivery or in catalyst.

Declaration of Competing Interest

The group declares no conflict of interest.

Acknowledgments

The group thanks Christelle Boscagli from the Centre Commun de Microscopie Appliquée (CCMA, Université Côte d'Azur) for the preparation of the substrates necessary for the SEM analyses. IR analyses were performed at the Smart City Innovation centre (Université Côte d'Azur, IMREDD). The "Smart City Innovation centre" is a project funded by the European union with the European fund for regional development and co-funded by Métropole Nice Côte d'Azur, the département Alpes-maritimes, the région Sud Provence-Alpes-Côte and France for the "initiative d'excellence" (Investissements d'avenir). This work has been supported by CNRS GDR 2088 « BIOMIM ».

Author contribution

Yanis Levieux-Souid and Ananya Sathanikan did the monomer synthesis and surface characterization, François Orange did the EDX analyses, Thierry Darmanin did the electropolymerization process. Thierry Darmanin and Frédéric Guittard did the discussion part and wrote the manuscript.

Supplementary materials

Supplementary material associated with this article can be found, in the online version, at doi:10.1016/j.electacta.2020.137677.

References

[1] W. Wei, G. Oltean, C.-.W. Tai, K. Edström, F. Björefors, L. Nyholm, High energy and power density TiO_2 nanotube electrodes for 3D Li-ion microbatteries, J. Mater. Chem. A 1 (2013) 8160–8169.
[2] O.O. Adisa, B.J. Cox, J.M. Hill, Methane storage in molecular nanostructures, Nanoscale 4 (2012) 3295–3307.
[3] H. Zhu, H. Chen, J. Wang, Q. Li, Fabrication of Au nanotube arrays and their plasmonic properties, Nanoscale 5 (2013) 3742–3746.
[4] C. Wang, K. Takei, T. Takahashi, A. Javey, Carbon nanotube electronics – moving forward, Chem. Soc. Rev. 42 (2013) 2592–2609.
[5] B. Su, Y. Tian, L. Jiang, Bioinspired interfaces with superwettability: from materials to chemistry, J. Am. Chem. Soc. 138 (2016) 1727–1748.
[6] F. Zhang, Z. Guo, Mater. Adv., Bioinspired Materials For Water-Harvesting: Focusing on Microstructure Designs and the Improvement of Sustainability, DOI, 2020, doi:10.1039/D0MA00599A.

[7] F. Guo, Q. Wen, Y. Peng, Z. Guo, Simple one-pot approach toward robust and boiling-water resistant superhydrophobic cotton fabric and the application in oil/water separation, J. Mater. Chem. A 5 (2017) 21866–21874.
[8] T. Darmanin, F. Guittard, Superhydrophobic and superoleophobic properties in Nature, Mater. Today 18 (2015) 273–285.
[9] W. Barthlott, C. Neinhuis, Purity of the sacred Lotus, or escape from contamination in biological surfaces, Planta 202 (1997) 1–8.
[10] L. Ge, S. Sethi, L. Ci, P.M. Ajayan, A. Dhinojwala, Carbon nanotube-based synthetic gecko tapes, Proc. Natl. Acad. Sci. U.S.A. 104 (2007) 10792–10795.
[11] G.D. Bixler, B. Bhushan, Fluid drag reduction and efficient self-cleaning with rice leaf and butterfly wing bioinspired surfaces, Nanoscale 5 (2013) 7685–7710.
[12] Z. Cheng, J. Gao, L. Jiang, Tip geometry controls adhesive states of superhydrophobic surfaces, Langmuir 26 (2010) 8233–8238.
[13] K.K.S. Lau, J. Bico, K.B.K. Teo, M. Chhowalla, G.A.J. Amaratunga, W.I. Milne, G.H. McKinley, K.K. Gleason, Superhydrophobic carbon nanotube forests, Nano Lett. 3 (2003) 1701–1705.
[14] H.-A. Lin, S.-C. Luo, B. Zhu, C. Chen, Y. Yamashita, H.-h. Yu, Molecular or nanoscale structures? The deciding factor of surface properties on functionalized poly(3,4-ethylenedioxythiophene) nanorod arrays, Adv. Funct. Mater. 23 (2013) 3212–3219.
[15] L. Lee, S.J. Park, Porous anodic aluminum oxide: anodization and templated synthesis of functional nanostructures, Chem. Rev. 114 (2014) 7487–7556.
[16] A. Fakhry, H. Cachet, C. Debiemme-Chouvy, Mechanism of formation of templateless electrogenerated polypyrrole nanostructures, Electrochim. Acta 179 (2015) 297–303.
[17] C. Debiemme-Chouvy, A. Fakhry, F. Pillier, Electrosynthesis of polypyrrole nano/micro structure using an electrogenerated oriented polypyrrole nanowire array as framework, Electrochim. Acta 268 (2018) 66–72.
[18] L. Qu, G. Shi, F. Chen, J. Zhang, Electrochemical growth of polypyrrole microcontainers, Macromolecules 36 (2003) 1063–1067.
[19] S. Gupta, Hydrogen bubble-assisted syntheses of polypyrrole micro/nanostructures using electrochemistry: structural and physical property characterization, J. Raman Spectrosc. 39 (2008) 1343–1355.
[20] J.T. Kim, S.K. Seol, J.H. Je, Y. Hwu, G. Margaritondo, The microcontainer shape in electropolymerization on bubbles, Appl. Phys. Lett. 94 (2009) 034103.
[21] T. Darmanin, F. Guittard, A one-step electrodeposition of homogeneous and vertically aligned nanotubes with parahydrophobic properties (high water adhesion), J. Mater. Chem. A 4 (2016) 3197–3203.
[22] C.R. Szczepanski, I. M'Jid, T. Darmanin, G. Godeau, F. Guittard, A template-free approach to nanotube-decorated polymer surfaces using 3,4-phenylenedioxythiophene (PhEDOT) monomers, J. Mater. Chem. A 4 (2016) 17308–17323.
[23] O. Sane, A. Diouf, G. Morán Cruz, F. Savina, R. Méallet-Renault, S. Amigoni, S.Y. Dieng, F. Guittard, T. Darmanin, Coral-like nanostructures, Mater. Today 31 (2019) 119–120.
[24] T. Darmanin, E.L. Klimareva, I. Schewtschenko, F. Guittard, I.F. Perepichka, Exceptionally strong effect of small structural variations in functionalized 3,4-phenylenedioxythiophenes on the surface nanostructure and parahydrophobic properties of their electropolymerized films, Macromolecules 52 (2019) 8088–8102.
[25] E.h.Y. Thiam, A. Dramé, S. Sow, A. Sene, C.R. Szczepanski, S.Y. Dieng, F. Guittard, T. Darmanin, Designing nanoporous membranes through templateless electropolymerization of thieno[3,4-b]thiophene derivatives with high water content, ACS Omega 4 (2019) 13080–13085.
[26] S. Bai, Q. Hu, Q. Zeng, M. Wang, L. Wang, Variations in surface morphologies, properties, and electrochemical responses to nitro-analyte by controlled electropolymerization of thiophene derivatives, ACS Appl. Mater. Interfaces 10 (2018) 11319–11327.
[27] D. Patra, C.-C. Chiang, W.-A. Chen, K.-H. Wei, M.-C. Wu, C.-W. Chu, Solution-processed benzotrithiophene-based donor molecules for efficient bulk heterojunction solar cells, J. Mater. Chem. A 1 (2013) 7767–7774.
[28] Y.-K. Peng, K.-M. Lee, C.-C. Ting, M.-W. Hsu, C.-Y. Liu, Making benzotrithiophene derivatives dopant-free for Perovskite solar cells: step-saving installation of π-spacers by a direct C–H arylation strategy, J. Mater. Chem. A 7 (2019) 24765–24770.
[29] H. Wei, J. Ning, X. Cao, X. Li, L. Hao, Benzotrithiophene-based covalent organic frameworks: construction and structure transformation under ionothermal condition, J. Am. Chem. Soc. 140 (2018) 11618–11622.
[30] C.B. Nielsen, J.M. Fraser, B.C. Schroeder, J. Du, A.J.P. White, W. Zhang, I. McCulloch, Benzotrithiophene - a planar, electron-rich building block for organic semiconductors, Org. Lett. 13 (2011) 2414–2417.
[31] I. Bousrih, M.El Kateb, C.R. Szczepanski, M. Beji, F. Guittard, T. Darmanin, A bioinspired strategy for designing well-ordered nanotubular structures by templateless electropolymerization of thieno[3,4-b]thiophene-based monomers, Philos. Trans. R. Soc. A 378 (2020) 20190450.
[32] A. Gbilimou, T. Darmanin, G. Godeau, F. Guittard, A templateless electropolymerization approach to nanorings using substituted 3,4-naphthalenedioxythiophene (NaPhDOT) monomers, ChemNanoMat 4 (2018) 140–147.
[33] G. Ramos Chagas, T. Darmanin, G. Godeau, F. Guittard, Nanocups and hollow microspheres formed by a one-step and templateless electropolymerization of thieno[3,4-*b*]thiophene derivatives as a function of the substituent, Electrochim. Acta 269 (2018) 462–478.
[34] G. Ramos Chagas, X. Xie, T. Darmanin, K. Steenkeste, A. Gaucher, D. Prim, R. Méallet-Renault, G. Godeau, S. Amigoni, F. Guittard, Electrodeposition of polypyrenes with tunable hydrophobicity, water adhesion and fluorescence properties, J. Phys. Chem. C 120 (2016) 7077–7087.
[35] A. Ringk, A. Lignie, Y. Hou, H.N. Alshareef, P.M. Beaujuge, Electropolymerized star-shaped benzotrithiophenes yield π-conjugated hierarchical networks with high areal capacitance, ACS Appl. Mater. Interfaces 8 (2016) 12091–12100.
[36] M.L. Keshtov, A.R. Khokhlov, S.A. Kuklin, F.C. Chen, E.N. Koukaras, G.D. Sharma, New D-A1–D-A2-type regular terpolymers containing benzothiadiazole and benzotrithiophene acceptor units for photovoltaic application, ACS Appl. Mater. Interfaces 8 (2016) 32998–33009.
[37] X. Guo, S.R. Puniredd, M. Baumgarten, W. Pisula, K. Müllen, Rational design of benzotrithiophene-diketopyrrolopyrrole-containing donor-acceptor polymers for improved charge carrier transport, Adv. Mater. 25 (2013) 5467–5472.
[38] T. Young, An essay on the cohesion of fluids, Philos. Trans. R. Soc. Lond. 95 (1805).
[39] D.K. Owens, R.C. Wendt, Estimation of the surface free energy of polymers, J. Appl. Polym. Sci 13 (1969) 1741–1747.
[40] R.N. Wenzel, Resistance of solid surfaces to wetting by water, Ind. Eng. Chem. 28 (1936) 988–994.
[41] A.B.D. Cassie, S. Baxter, Wettability of porous surfaces, Trans. Faraday Soc. 40 (1944) 546–551.
[42] A. Marmur, Hydro- hygro- oleo- omni-phobic? Terminology of wettability classification, Soft Matter 8 (2012) 6867–6870.
[43] L. Feng, Y. Zhang, J. Xi, Y. Zhu, N. Wang, F. Xia, L. Jiang, Petal effect: a superhydrophobic state with high adhesive force, Langmuir 24 (2008) 4114–4119.
[44] B. Bhushan, M. Nosonovsky, The rose petal effect and the modes of superhydrophobicity, Philos. Trans. R. Soc. A 368 (2010) 4713–4728.
[45] C.R. Szczepanski, T. Darmanin, F. Guittard, Recent advances in the study and design of parahydrophobic surfaces: from natural examples to synthetic approaches, Adv. Colloid Interface Sci. 241 (2017) 37–61.